Analyzing solution-phase time-resolved x-ray diffraction data by isolated-solute models

Jae Hyuk Lee, Kyoung Hwan Kim, Tae Kyu Kim, Youhong Lee, and Hyotcherl Ihee[a)]
Department of Chemistry, Korea Advanced Institute of Science and Technology (KAIST), Daejeon 305-701, Republic of Korea and School of Molecular Science (BK21), Korea Advanced Institute of Science and Technology (KAIST), Daejeon 305-701, Republic of Korea

(Received 2 August 2006; accepted 9 October 2006; published online 6 November 2006)

Extracting transient structural information of a solute from time-resolved x-ray diffraction (TRXD) data is not trivial because the signal from a solution contains not only the solute-only term as in the gas phase, but also solvent-related terms. To obtain structural insights, the diffraction signal in q space is often Fourier sine transformed (FT) into r space, and molecular dynamics (MD) simulation-aided signal decomposition into the solute, cage, and solvent terms has so far been indispensable for a clear-cut assignment of structural features. Here we present a convenient method of comparative structural analysis without involving MD simulations by incorporating only isolated-species models for the solute. FT is applied to both the experimental data and candidate isolated-solute models, and comparison of the correlation factors between the experimental FT and the model FTs can distinguish the best candidate among isolated-solute models for the reaction intermediates. The low q region whose influence by solvent-related terms is relatively high can be further excluded, and this mode of truncated Fourier transform (TFT) improves the correlation factors and facilitates the comparison. TFT analysis has been applied to TRXD data on the photodissociation of $C_2H_4I_2$ in two different solvents (methanol and cyclohexane), HgI_2 in methanol, and I_3^- in methanol excited at 267 nm. The results are consistent with previous conclusions for $C_2H_4I_2$ in methanol and HgI_2 in methanol, and the new TRXD data reveal that the C_2H_4I transient radical has a bridged structure in cyclohexane and I_3^- in methanol decomposes into $I+I_2^-$ upon irradiation at 267 nm. This TFT method should greatly simplify the analysis because it bypasses MD simulations. © *2006 American Institute of Physics*. [DOI: 10.1063/1.2386158]

I. INTRODUCTION

Recent years have witnessed great advances in ultrafast diffraction using either x-rays[1–26] or electrons.[27–29,29–42] In particular, time-resolved x-ray diffraction (TRXD) from laser-excited molecules in liquids has been realized[9–14] due to the development of global fitting analysis[12] and technological innovations[10,43] in synchrotron instrumentation, and has made it possible to track complex reactions in solution by time-resolved diffraction with temporal and spatial resolutions of 100 ps and 0.001 Å, respectively. For instance, the photodissociation reaction of HgI_2 in methanol was recently investigated by this technique and the data analysis revealed that the major primary reaction is a simple two-body dissociation giving HgI+I, whereas the three-body dissociation giving Hg+I+I is negligible, in stark contrast to the gas phase reaction which gives both channels.[14] In addition, it was shown that the formation of the HgI–I isomer is also negligible. Moreover, TRXD allowed for the properties and structures of elemental liquids to be studied.[15–17]

Compared with obtaining structural information from the gas phase,[27,28,40,41,44–46] obtaining like information from the solution phase is more difficult due to the presence of a large number of solvent molecules that surround the solute molecules of interest. The diffraction signal in the gas phase comes only from isolated (noninteracting) molecules (solutes),[27,37,41,47–49] but the diffraction signal in solution is the sum of the solute-only term, the solute-solvent cross term, and the solvent-only term. Due to this complexity, fingerprinting of the reaction intermediates and the mathematical decomposition of the scattered x-ray signal has so far been aided by quantum calculations and molecular dynamics (MD) simulations.[12] MD simulation can generate statistical atom-atom correlation functions for a solution[50,51] and has been indispensable for disentangling the different contributions from the scattering patterns.

However, obtaining all MD components for a complete global fitting analysis is time consuming and the accuracy of the MD simulation in low q region is often questionable due to the use of a finite simulation box size and an approximate potential. In addition, the knowledge of the structural dynamics of the solute alone would be the first step to solve the interesting chemistry/physics of solvent-solute interactions, and the molecular structures of the intermediate species are themselves the target of research. For example, it is of great interest to determine whether the C_2H_4I radical is bridged or not in the photodissociation of I from $C_2H_4I_2$ in solution, as shown in Fig. 1(a) because the structural nature of the transient radical determines the stereochemistry of the final products. The solvent heating and expansion is a secondary problem. Another example is the photodissociation of HgI_2 in

[a)]Electronic mail: hyotcherl.ihee@kaist.ac.kr

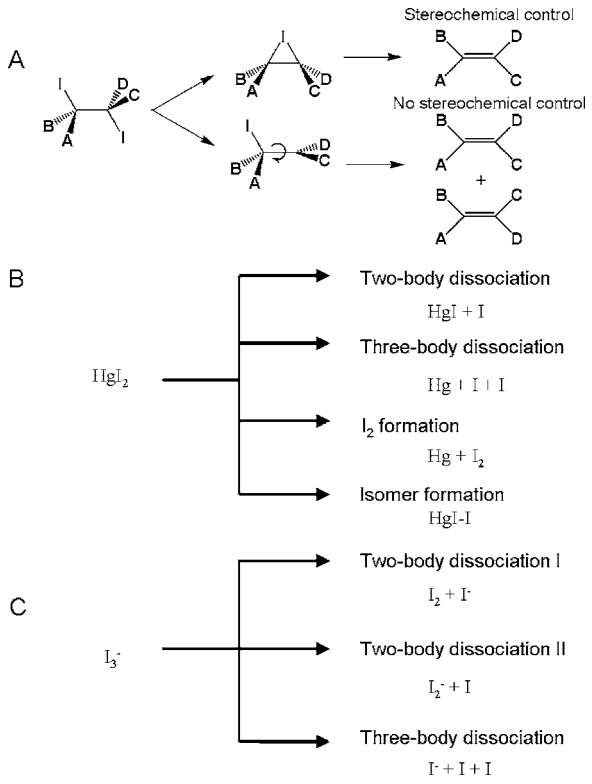

FIG. 1. Three problems of interest. (A) The relationship between the structure of intermediates and stereochemical control in the final products in the iodine elimination reaction of $C_2H_4I_2$ in solution. In this work, the reaction intermediates in both polar (methanol) and nonpolar (cyclohexane) solvents are considered. The bridged structure ensures stereochemical control, whereas the classical *anti* structure does not. (B) The photodissociation of HgI_2 in solution. Four candidate reaction channels are considered. (C) The photodissociation of I_3^- in solution. Three candidate reaction channels are considered.

solution, which has four candidate reaction channels as shown in Fig. 1(b). In this paper, we also investigated the photodissociation of I_3^- in methanol, as shown in Fig. 1(c). Note that the solute-only term can be generated by considering structural information of only a single isolated solute molecule (an isolated-solute model analogous to a gas-phase model) rendering MD simulations unnecessary. For this reason, an alternative way to analyze time-resolved diffraction data using only isolated-solute model without involving time-consuming MD simulations is desirable.

To obtain structural insight, the diffraction signal in q space is often Fourier sine transformed (FT) into r-space data, radial distribution functions (RDFs). Here we present a new method of obtaining structural insight by incorporating isolated-solute models without biasing the experimental data towards candidate models. The key idea is simple; FT is applied to both the experimental data and candidate isolated-solute models, and a comparison of the degree of correlation between the experimental RDF and the model RDFs can distinguish the best candidate among isolated-solute models for the reaction intermediates. For the solute containing heavy atoms, which scatter to much larger q values, the high q region is dominated by the solute since the light-atom scattering of the solvent falls off more rapidly with q. The low q region whose influence by solvent-related terms is relatively high can be further excluded, and this mode of truncated Fourier transform (TFT) improves the degree of correlation and facilitates the comparison since it allows for the experimental data to be uncontaminated by a theoretical model, while still being able to be used to evaluate candidate isolated-solute models. The application of TFT to TRXD data on the photodissociation of $C_2H_4I_2$ in methanol and cyclohexane clearly shows that the C_2H_4I transient radical has a bridged structure rather than a classical *anti* structure, confirming the previous conclusion.[12] Also in the case of HgI_2 and I_3^-, TFT analysis can distinguish the best reaction channel against other candidate models. TFT analysis should greatly simplify the analysis since MD simulations are not required. TFT is relevant not only to solution-phase data but also to gas-phase data[27,28,40,41] because the low q region (below 2–4 $Å^{-1}$) of the latter is typically not obtained experimentally.

We explain the experimental method in Sec. II. In Sec. III, we show two modes of truncating the low q signal in Fourier transform and their effects in a model system. Then, the developed method is applied to real experimental data of $C_2H_4I_2$, HgI_2, and I_3^- in solution.

II. EXPERIMENT

Experimental details are provided in our previous publications.[12,14,16,52] Time-resolved data on I_3^- in methanol and $C_2H_4I_2$ in cyclohexane were newly collected, but the data sets for $C_2H_4I_2$ and HgI_2 in methanol were taken from our previous publication[12,14] for analysis here. Difference-diffraction curves ($\Delta S(q,t)$, [$q=(4\pi/\lambda)\sin(\theta)$, where λ is the wavelength of the x rays, 2θ is the scattering angle, and t is the time delay]) were generated by subtracting the reference data at −3 ns from the data at any other time delay.[11] We often multiply $\Delta S(q,t)$ by the scattering vector, q, to magnify the intensity at higher q which is dominated by the solute-only term. The possible structures of the parent molecules and the transient intermediates in the solution phase were calculated by the *ab initio* and density functional theory (DFT) methods using the code GAUSSIAN 03.[53] The details are provided clearly in our previous publications.[42,54]

III. RESULTS AND DISCUSSION

A. Truncated Fourier transform

Since the result in q space is abstract, one often presents the result more conveniently in r space. The corresponding difference RDF, $r\Delta S(r,t)$, which provides radial electron density changes as a function of interatomic distance r, is obtained by sine-Fourier-transforming the $q\Delta S(q,t)$ curves,

$$r\Delta S(r,t) = \frac{1}{2\pi^2}\int_0^\infty q\Delta S(q,t)\sin(qr)dq. \quad (1)$$

Often we multiply some modification function $M(q)$ to $q\Delta S(q,t)$. $M(q)$ can be simply $\exp(-\alpha q^2)$ or further divided by a sharpening function where the constant α is a damping constant to account for the fact that the experimental data do not extend to infinity. The damping factor is chosen so that $\exp(-\alpha q^2)$ at the maximum value of q is close to 0.1. In our case this corresponds to 0.03 $Å^2$. To absorb the modification

function, one can redefine $r\Delta S(r,t)$ as the sine-Fourier transform (SFT) of $f(q,t)=q\Delta S(q,t)M(q)$,

$$r\Delta S(r,t)=\frac{1}{2\pi^2}\int_0^\infty f(q,t)\sin(qr)dq. \tag{2}$$

Because of the absence of experimental points in the low q region, one normally fills the gap with theoretical curves to extend the data and in this way can minimize the truncation in the FT.[55–57] In this process, the resulting r-space curves are biased toward the attached theoretical model. This model bias can hamper the validity of comparing the experimental data to candidate theoretical models in r space.

Since the solvent-related contribution to $\Delta S(q,t)$ is relatively high in the low q region, it can be reduced by removing the low q part of $\Delta S(q,t)$ before FT. The simplest way (mode A) is to append zero values to $\Delta S(q,t)$ for $0\leqslant q\leqslant q_T$ and to transform from q_T rather than zero. Then the corresponding TFT can be defined as follows:

$$r\Delta S^A(r,t)=\frac{1}{2\pi^2}\int_{q_T}^\infty f(q,t)\sin(qr)dq. \tag{3}$$

If we define a step function $u(q)=0$ for $|q|<q_T$ and 1 for $|q|>q_T$, and a window function $w(q)=1$ for $|q|<q_T$ and 0 for $|q|>q_T$, $r\Delta S^A(r,t)$ can be considered as SFT of the original function multiplied by the step function. Then, $r\Delta S^A(r,t)$ is the convolution of $r\Delta S(r,t)$ and $U(r)$, the cosine-Fourier transform (CFT) of $u(q)$. Alternatively $r\Delta S^A(r,t)$ can be obtained by subtracting the convolution of $r\Delta S(r,t)$ and $W(r)$, the CFT of $w(q)$, from $r\Delta S^A(r,t)$ (see Appendix A for details)

$$\begin{aligned} r\Delta S^A(r,t)&=(r\Delta S(r,t))\otimes U(r)\\ &=r\Delta S(r,t)-(r\Delta S(r,t))\otimes W(r), \end{aligned} \tag{4}$$

where the symbol $\otimes$ means convolution. The term $(r\Delta S(r,t))\otimes W(r)$ corresponds to the contribution of the low q region alone. Subtracting this from the original $r\Delta S(r,t)$ removes the low q contribution, but at the same time, $W(r)$ has the $\sin(q_Tr)/r$ component and thus creates serious ripples in the resulting RDFs, as can be seen in the following section. This truncation error can be eliminated by shifting $f(q,t)$ by q_T and this offers an alternative way to truncate the low q data below q_T (mode B) as in

$$r\Delta S^B(r,t)=\frac{1}{2\pi^2}\int_0^\infty f(q+q_T,t)\sin(qr)dq. \tag{5}$$

If we define a signum function, $\mathrm{sgn}(q)=-1$ for $q<0$ and 1 for $q>0$, $r\Delta S^B(r,t)$ can be expressed as follows (see Appendix B for details):

$$\begin{aligned} r\Delta S^B(r,t)&=\cos(q_Tr)(r\Delta S(r,t))\\ &\quad-(\sin(q_Tr)r\Delta S(r,t))\otimes \mathrm{SGN}Y(r), \end{aligned} \tag{6}$$

where $\mathrm{SGN}Y(r)$ is the SFT of $\mathrm{sgn}(q)$. Since $\mathrm{SGN}Y(r)$ is simply proportional to $1/r$, which is a smooth function without oscillations, the convolution does not introduce ripples. However, the multiplicative $\cos(q_Tr)$ and $\sin(q_Tr)$ terms change the phase of the original $r\Delta S(r,t)$.

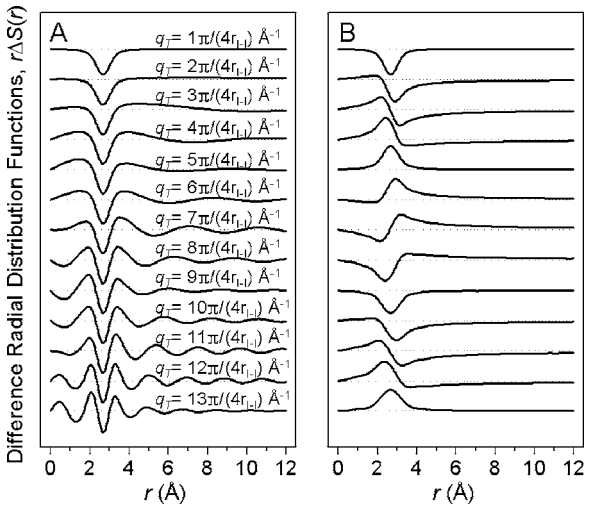

FIG. 2. Truncated Fourier transform applied to a model system of the dissociation of I_2 with $r_{I-I}=2.67$ Å into two iodine atoms ($I_2\rightarrow I+I$). Each panel shows the $r\Delta S(r)$ curves as a function of q_T. Panels (A) and (B) are from using modes A and B, respectively. Truncation errors (ripples) are serious in mode A, but disappear in mode B. Instead, the phase of the peak changes as a function of q_T in mode B.

The differences between the two TFTs in Eqs. (3) and (5) can be visualized by applying them to a model system as done in the next section. It will be shown that mode B is useful for visual (qualitative) comparison (Secs. III B and III C), but both modes give the same quantitative results (Sec. III D).

B. Application to a model system

Truncation inevitably introduces distortions in the resulting RDF. However, the distortions are not the real handicap as far as both the experimental data and the theoretical model are treated by the same TFT in a comparative structural analysis because the introduced distortions are the same. As far as the distortions do not hamper the comparison between the experiment and theory, the resulting TFTs can still be useful in differentiating several candidate theoretical models against the experimental data. To gauge the effect of truncation in each mode outlined in the previous section, dissociation of I_2 molecule with the I–I distance of 2.67 Å into two iodine atoms ($I_2\rightarrow I+I$) was used as a model system. Figure 2 shows the RDFs from two different ways of TFT as a function of q_T. It is evident that the ripples, often called truncation errors, become a serious problem in mode A. By contrast, mode B does not introduce any ripples, but instead the phase of the peak changes as a function of q_T. For example, the peak turns positive at $q_T=\pi/r_{I-I}$ Å^{-1} and reverses to negative at $q_T=2\pi/r_{I-I}$ Å^{-1}. When $q_T=\frac{1}{2}\pi/r_{I-I}$ Å^{-1} and $q_T=\frac{3}{2}\pi/r_{I-I}$ Å^{-1}, differential forms of the peak appear. The fact that the phase of the peak corresponding to an internuclear distance r returns to its original phase when $q_T=2\pi/r$ Å^{-1} becomes important when one assigns the peak based on the assignments at $q_T=0$ Å^{-1}.

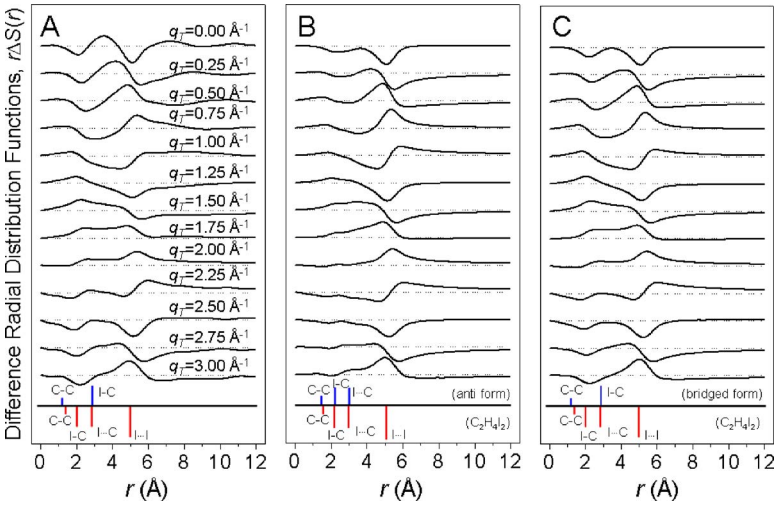

FIG. 3. TFT with mode *B* of $C_2H_4I_2$/methanol data at 100 ps (A), gas-phase models of the *anti* structure (B), and the bridged structure (C). At the bottom of each graph, peak assignments are given for the disappearing parent molecule (below the horizontal line) and the appearing intermediate structure (above the horizontal line). The position of a bar is related to the corresponding internuclear distance and the height is proportional to the number of the corresponding internuclear distance. Qualitative comparison clearly indicates that the experimental TFT agrees well with the TFT of the bridged model rather than the *anti* model.

C. Application to experimental data I: $C_2H_4I_2$ in methanol

TFT analysis would be useful only when it can offer structural insight for real data. To test its usefulness, it was applied to real data of $C_2H_4I_2$ in two different solvents, methanol and cyclohexane. The photodissociation reaction of $C_2H_4I_2$ in methanol was recently investigated by TRXD,[12] but that in a nonpolar solvent (cyclohexane) has not been investigated yet. One of the most important issues was the structural identity of the C_2H_4I radical; whether it is a bridged form or a classical *anti* structure as illustrated in Fig. 1. Mathematical decomposition via MD simulation revealed that the bridged structure, not the *anti* structure, agrees much better with the experimental data at 100 ps.[12] Therefore, it is of great interest if TFT analysis, which does not require MD simulation, can discern which model better explains the experimental data at 100 ps and which model explains the experimental data in cyclohexane better.

We applied two modes of TFT to the $C_2H_4I_2$/methanol data at 100 ps. TFT is applied to the $q\Delta S(q,t)$ curves of the experimental data and gas-phase models (in this case, the bridged and the *anti* structure). For each case, the resulting RDFs are displayed as a function of q_T. As expected, spurious ripples in mode *A* (not shown) make visual (qualitative) comparison of the experimental data to two candidate structural models difficult. In the case of mode *B* shown in Fig. 3, it is quite a different story. Throughout all q_T ranges above 1 Å^{-1}, the RDFs from the bridged model show clearly different features from those of the *anti* model, especially around 2 Å, which is sensitive to the C–I bond distance. This peak can be used as a fingerprint region because the bridged structure has two identical C···I internuclear distances, whereas the *anti* structure has two different C···I internuclear distances. Comparison of the experimental TFT and two theoretical TFTs instantly reveals that the experimental data agree much better with the bridged model than with the *anti* model. When q_T is larger than 1 Å^{-1}, the experimental RDFs are almost identical to the corresponding RDFs of the bridged model. The RDFs of the *anti* model reproduce the experimental peak around 5 Å, but fail around 2 Å. The peak at 5 Å is due to the depletion of I···I internuclear pair in the parent molecule and is common for both channels producing either the bridged radical or the *anti* radical. It should be noted that the negative peak corresponding to the I···I internuclear distance (r=5 Å) becomes negative again at $q_T = 2\pi/r \approx 1.25$ Å^{-1} and $4\pi/r \approx 2.50$ Å^{-1}. In the same way, the negative peak at ca. 2.0 Å obtains its original phase at $2\pi/r \approx 3$ Å^{-1}. Therefore, the application of TFT with mode *B* to TRXD data on the photodissociation of $C_2H_4I_2$ in methanol clearly shows that the C_2H_4I transient radical has a bridged structure rather than a classical *anti* structure, confirming the previous conclusion.[12]

D. Structural correlation factors

The comparative analysis of experimental data to theoretical models using TFT described in the previous section relies on visual comparison and is therefore rather qualitative. A quantitative tool can be provided by using structural correlation factors between the experimental TFT and the TFT of the theoretical model defined as follows:

$$C(t) = \int (r\Delta S^{\mathrm{exp}}(r,t) \cdot r\Delta S^{\mathrm{model}}(r,t))dr, \tag{7}$$

where $r\Delta S^{\mathrm{expt}}(r,t)$ is the experimental RDF and $r\Delta S^{\mathrm{model}}(r,t)$ is the RDF of an isolated-solute model. It is important that both experimental and model RDFs should be normalized so that

$$\int (r\Delta S(r,t))^2 dr = 1. \tag{8}$$

This normalization ensures that the correlation factors approach unity for a perfect model. In addition, this makes the experimental data scaled to theoretical models even when the exact population of the transient concentration is not known.

Figure 4 shows the correlation factors for the case of $C_2H_4I_2$ in methanol data as a function of q_T for both modes *A* and *B*. Comparison of the *anti* and bridged model shows that the correlation factors of the bridged model are always closer to 1 than those of the *anti* model, consistent with the qualitative analysis. It should be noted that both modes *A* and *B* give almost the same plots and either mode should be fine

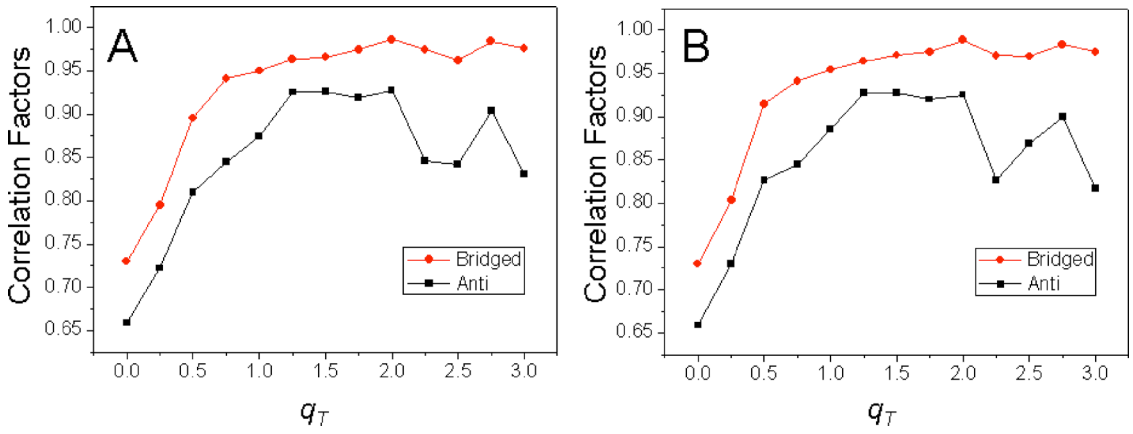

FIG. 4. Structural correlation factors of the experimental TFT data to theoretical models as a function of q_T for the TRXD data of $C_2H_4I_2$ in methanol. Panels (A) and (B) are from using modes *A* and *B*, respectively, although they are almost identical. In general, structural correlation factors to the bridged structure are higher than those to the *anti* structure, quantitatively indicating the former explains the experimental data better.

for a quantitative comparison. The two modes of truncation presented in this paper are not special ones but rather typical and natural choices. If the truncation mode affects the correlation factors, it would be problematic. The important point is that the experimental data and the theoretical models are transformed in the exact same way. Note that the correlation factor at $q_T=0$ (i.e., without truncation) already allows one to distinguish reaction pathways. The correlation factors increase with increasing q_T due to the reduced contribution from solvent and comparing correlations factors in a wider range of q_T adds discriminating power.

E. Application to experimental data II: ($C_2H_4I_2$) in cyclohexane

The data collected for the same solute ($C_2H_4I_2$) in two different solvents (methanol and cyclohexane) provide an excellent opportunity to evaluate the validity of TFT analysis. We applied TFT analysis to TRXD data in cyclohexane. The data in cyclohexane at 50 ps have a worse signal-to-noise ratio than that in methanol. When q_T increases, the contribution from solvent decreases and the RDFs from two different solvents become very similar other than more ripples due to lower signal-to-noise ratio, indicating the transient solute structure is the same, regardless of the solvent (not shown). Comparison of the RDFs from $C_2H_4I_2$/cyclohexane (not shown) to the TFT of theoretical models clearly shows that the experimental data agree much better with the bridged model than the *anti* model. Figure 5 shows a plot of the correlation factors for both models and it is evident that those for the bridged model are much closer to 1 than those of the *anti* model. It should be noted that MD simulations have not been applied for $C_2H_4I_2$/cyclohexane, but TFT analysis can still distinguish which model explains the experimental data and led us to conclude that the bridged C_2H_4I radical forms regardless of solvent polarity.

F. Application to experimental data III: HgI_2 in methanol

Determining the reaction channel in the photodissociation of HgI_2 in methanol is more complicated since four candidate channels exist. In the global fitting analysis using MD simulations, these four channels were compared with experimental data (Fig. 5 of Ref. 14) and the simple two-body dissociation channel ($HgI_2 \rightarrow HgI+I$) gave the best experimental agreement. From TFT of HgI_2/methanol data at 100 ps and isolated-solute models of four candidate channels (not shown), the isomer formation channel can be immediately rule out, but other candidate channels except the isomer channel yield similar RDFs and thus make the qualitative comparison difficult. However, quantitative comparison based on the correlation factors shown in Fig. 6 clearly shows that the two-body dissociation ($HgI_2 \rightarrow HgI+I$) is the dominant reaction channel over other candidate channels. The correlation factor for the two-body dissociation is already close to 1 even at $q_T=0$. This is because the solvent contribution is not so severe compared to the solute signal at low q due to the heavy atoms in the solute molecule.

G. Application to experimental data IV: I_3^- in methanol

We applied TFT analysis to new experimental data on I_3^- in methanol. Photodissociation of I_3^- has been extensively studied using time-resolved spectroscopy.[58–60] Previous stud-

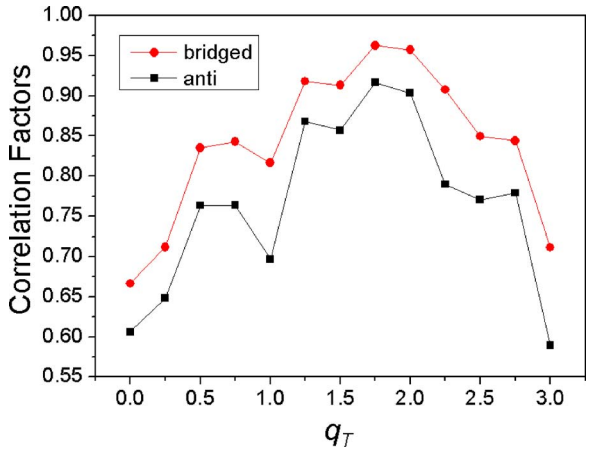

FIG. 5. Structural correlation factors of the experimental TFT data for the two theoretical models of C_2H_4I as a function of q_T for TRXD data at 50 ps of $C_2H_4I_2$ in cyclohexane. In general, structural correlation factors for the bridged structure are higher than those for the *anti* structure, quantitatively indicating the former explains the experimental data better.

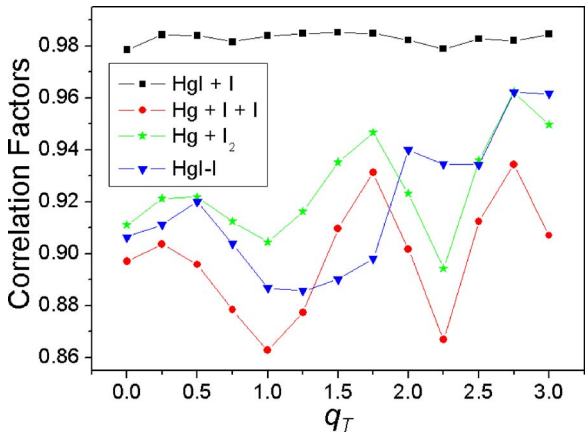

FIG. 6. Structural correlation factors of the experimental TFT data of HgI_2/methanol data at 100 ps to gas-phase models of four candidate channels; HgI+I, Hg+I+I, Hg+I_2, and HgI–I isomers as a function of q_T. In general, structural correlation factors to the two-body dissociation channel are higher than those for other reaction candidate channels, quantitatively indicating the former explains the experimental data better.

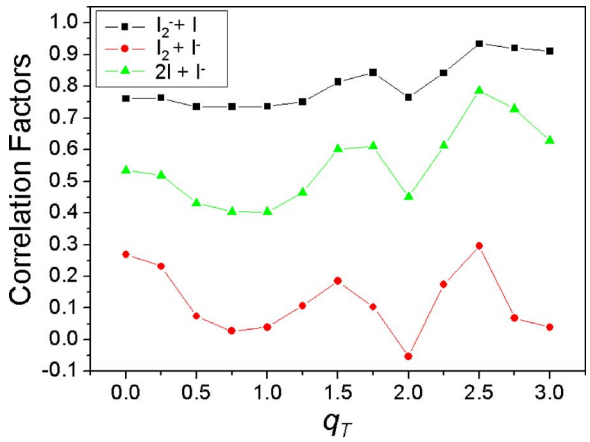

FIG. 7. Structural correlation factors of the experimental TFT data of I_3^- in methanol at 100 ps to gas-phase models of three candidate channels; $I+I_2^-$, I^-+I_2, and I^-+I+I as a function of q_T. In general, structural correlation factors of the two-body dissociation channel are higher than those for other reaction candidate channels, quantitatively indicating the former is the dominant reaction pathway in the photodissociation I_3^- in methanol upon 267 nm excitation.

ies suggest three candidate reaction channels which depend on the excitation wavelength [Fig. 1(c)]. The nature of the simple two-body dissociation channel ($I_3^- \rightarrow I_2^- + I$) in the solution was well established by Banin and Ruhman.[58] Kuhne and Vohringer reported the possibility of the existence of the three-body dissociation channel ($I_3^- \rightarrow 2I + I^-$) when the laser energy was high enough.[59] In the gas phase, Zanni *et al.* detected the 1:2 mass channel and 1:1 mass channel, which correspond to the two-body and three-body dissociation channels, respectively.[60] The two-body dissociation channel can be either a ($I_3^- \rightarrow I_2^- + I$) channel or a ($I_3^- \rightarrow I_2 + I^-$) channel, and the three-body dissociation channel is $I_3^- \rightarrow I + I + I^-$.

We applied mode *B* to the recently collected TRXD data for I_3^- in methanol. From the RDFs of I_3^-/methanol data at 100 ps and three candidate channels (not shown), it can be seen that only the I_2^- formation channel has a similar pattern to the experimental data because I_2^- has a longer bond length. This indicates that I_3^- dissociates into I_2^- and I rather than other candidate channels. Quantitative analysis using correlations factors shown in Fig. 7 can discriminate three channels more dramatically. The correlation factors of the I_2^- formation channel at various q_T values are much higher than others. This quantitatively indicates that the I_2^- formation channel is the dominant reaction pathway over other candidate channels from photodissociation of I_3^- at 267 nm.

IV. CONCLUSIONS

A new method of obtaining structural insight by incorporating only isolated-solute models, which does not bias the experimental data, is presented. FT is applied to both the experimental data and candidate isolated-solute models, and comparison of the correlation factors between the experimental FT and the model FTs can distinguish the best among candidate models for the reaction intermediates. The low q region whose influence by solvent-related terms is relatively high can be further excluded, and this mode of truncated Fourier transform (TFT) improves the correlation factors and facilitates the comparison. This new method offers advantages in that the experimental data are not contaminated by any theoretical model, and can still be used to discriminate candidate isolated-solute models against the experimental data, thereby facilitating the comparison between the theory and experiment. The application of TFT analysis to TRXD data on the photodissociation of $C_2H_4I_2$ in two different solvents, methanol and cyclohexane, shows that the transient C_2H_4I radical is bridged in both polar and nonpolar solvents. TFT analysis also confirms that the major primary reaction channel for the photodissociation of HgI_2 in methanol is two-body dissociation. TFT analysis of the TRXD data in methanol clearly shows that I_3^- photodissociates into $I+I_2^-$ rather than I^-+I_2 or I^-+2I. TFT analysis is simpler in that it does not require any MD simulations. TFT is relevant not only to solution-phase data as discussed in this paper but also to gas-phase data[27,28,40,41,44–46,55] because the low q region of the latter is typically not obtained experimentally.

ACKNOWLEDGMENTS

The authors are indebted to M. Wulff, S. Bratos, R. Vuilleumier, Q. Kong, M. Cammarata, M. Lo Russo, E. Pontecorvo, M. Lorenc, F. Schotte, P. A. Anfinrud, and A. Plech for their invaluable help with the theory and the experiments. This work was supported by the Korea Science and Engineering Foundation Nano R&D Program Grant No. 2005-02638 and Korea Research Foundation Grant funded by Korean Government (MOEHRD) (R08-2004-000-10076-0).

APPENDIX A: DERIVATION OF EQUATION (4)

In our application,

$$f(q,t) = q\Delta S(q,t)M(q), \tag{A1}$$

where $f(q,t)$ is defined only for $q>0$, but we can expand it as an odd function satisfying $f(-q,t)=-f(q,t)$.

Then,

$$r\Delta S(r,t) = \frac{1}{2\pi^2}\int_0^\infty f(q,t)\sin(qr)dq, \tag{A2}$$

$$f(q,t) = 4\pi\int_0^\infty r\Delta S(r,t)\sin(qr)dq. \tag{A3}$$

A step function can be defined as follows:

$$u(q) = 0 \quad \text{for } |q| < q_T \quad \text{and } 1 \quad \text{for } |q| > q_T \tag{A4}$$

and the CFT of $u(q)$ is[61]

$$U(r) = (2/\pi)^{1/2}\int_0^\infty u(q)\cos(qr)dq = (2\pi)^{1/2}\delta(r) - (2/\pi)^{1/2}\frac{\sin(q_T r)}{r}. \tag{A5}$$

The mode A in Eq. (3) can be expressed as follows:

$$\begin{aligned} r\Delta S^A(r,t) &= \frac{1}{2\pi^2}\int_{q_T}^\infty f(q,t)\sin(qr)dq \\ &= \frac{1}{2\pi^2}\int_0^\infty f(q,t)u(q)\sin(qr)dq \\ &= (2\pi)^{-1/2}\int_{-\infty}^\infty u\Delta S(u,t)U(r-u)du \\ &= (r\Delta S(r,t)) \otimes U(r), \end{aligned} \tag{A6}$$

where the symbol $\otimes$ means convolution after absorbing the constant. Equation (C13) gives a more detailed derivation.

A window function can be defined as

$$w(q) = 1 \quad \text{for } |q| < q_T \quad \text{and } 0 \quad \text{for } |q| > q_T \tag{A7}$$

and the CFT of $w(q)$ is as follows:[61]

$$W(r) = (2/\pi)^{1/2}\int_0^\infty w(q)\cos(qr)dq = (2/\pi)^{1/2}\frac{\sin(q_T r)}{r}. \tag{A8}$$

The mode A in Eq. (3) can be expressed as follows:

$$\begin{aligned} r\Delta S^A(r,t) &= \frac{1}{2\pi^2}\int_{q_T}^\infty f(q,t)\sin(qr)dq \\ &= \frac{1}{2\pi^2}\int_0^\infty f(q,t)(1-w(q))\sin(qr)dq \\ &= r\Delta S(r,t) - \frac{1}{2\pi^2}\int_0^\infty f(q,t)w(q)\sin(qr)dq \\ &= r\Delta S(r,t) - (r\Delta S(r,t)) \otimes W(r). \end{aligned} \tag{A9}$$

Combining Eqs. (A6) and (A8) gives

$$\begin{aligned} r\Delta S^A(r,t) &= (r\Delta S(r,t)) \otimes U(r) \\ &= r\Delta S(r,t) - (r\Delta S(r,t)) \otimes W(r), \end{aligned} \tag{A10}$$

which is Eq. (4).

APPENDIX B: DERIVATION OF EQUATION (6)

We define a signum function,

$$\mathrm{sgn}(q) = -1 \quad \text{for } q < 0 \quad \text{and } 1 \quad \text{for } q > 0. \tag{B1}$$

Then its FT is[61]

$$\mathrm{SGN}(r) = (2\pi)^{-1/2}\int_{-\infty}^\infty \mathrm{sgn}(q)\exp(-iqr)dq = -2(2/\pi)^{1/2}\frac{i}{r} \tag{B2}$$

and its sine-Fourier transform (SFT) is as follows:

$$\mathrm{SGN}Y(r) = (2/\pi)^{1/2}\int_0^\infty \mathrm{sgn}(q)\sin(qr)dq = (2\pi)^{-1/2}\int_{-\infty}^\infty \mathrm{sgn}(q)\sin(qr)dq = 2(2/\pi)^{1/2}\frac{1}{r}. \tag{B3}$$

Mode B in Eq. (5) can be expressed as follows:

$$\begin{aligned} r\Delta S^B(r,t) &= \frac{1}{2\pi^2}\int_0^\infty f(q+q_T,t)\sin(qr)dq \\ &= \frac{1}{2\pi^2}\int_{-\infty}^\infty f(q+q_T,t)\left(\frac{1}{2}+\frac{1}{2}\,\mathrm{sgn}(q)\right)\sin(qr)dq \\ &= \frac{1}{4\pi^2}\int_{-\infty}^\infty f(q+q_T,t)\sin(qr)dq \\ &\quad + \frac{1}{4\pi^2}\int_{-\infty}^\infty f(q+q_T,t)\mathrm{sgn}(q)\sin(qr)dq \\ &= \cos(q_T r)(r\Delta S(r,t)) \\ &\quad + \frac{1}{4\pi^2}\int_{-\infty}^\infty f(q+q_T,t)\mathrm{sgn}(q)\sin(qr)dq. \end{aligned} \tag{B4}$$

The relation in Eq. (C9) was used. The second term in the last line of Eq. (B4) is as follows:

$$\frac{1}{4\pi^2}\int_{-\infty}^{\infty} f(q+q_T,t)\mathrm{sgn}(q)\sin(qr)dq$$
$$= -\mathrm{Im}\left[\frac{1}{4\pi^2}\int_{-\infty}^{\infty} f(q+q_T,t)\mathrm{sgn}(q)\exp(-iqr)dq\right]$$
$$= -\mathrm{Im}\left[\frac{1}{4\pi^2}\int_{-\infty}^{\infty}\int_{-\infty}^{\infty} f(q+q_T,t)\exp(-iqu)dq\mathrm{SGN}(r-u)du\right]$$
$$= -\mathrm{Im}\left[\frac{1}{4\pi^2}\int_{-\infty}^{\infty} \exp(iq_Tu)\int_{-\infty}^{\infty} f(q,t)\exp(-iqu)dq\mathrm{SGN}(r-u)du\right]$$
$$= -\mathrm{Im}\left[\frac{1}{4\pi^2}\int_{-\infty}^{\infty} \exp(iq_Tu)\left(-2i\int_{0}^{\infty} f(q,t)\sin(qu)dq\right)\mathrm{SGN}(r-u)du\right]$$
$$= -\mathrm{Im}\left[-i\int_{-\infty}^{\infty} \exp(iq_Tu)u\Delta S(u,t)\mathrm{SGN}(r-u)du\right]$$
$$= -\int_{-\infty}^{\infty} \sin(q_Tu)u\Delta S(u,t)\mathrm{SGN}Y(r-u)du = -(\sin(q_Tr)r\Delta S(r,t))\otimes \mathrm{SGN}Y(r). \quad \text{(B5)}$$

Combining Eqs. (B4) and (B5) gives

$$r\Delta S^B(r,t) = \cos(q_Tr)(r\Delta S(r,t)) - (\sin(q_Tr)r\Delta S(r,t)) \otimes \mathrm{SGN}Y(r), \quad \text{(B6)}$$

which is Eq. (6).

APPENDIX C: FOURIER TRANSFORM RELATIONS USED IN APPENDIXES A and B

If $f(q)$, $F(r)$ and $g(q)$, $G(r)$ are two sets of Fourier transforms such that[56,61]

$$f(q) = (2\pi)^{-1/2}\int_{-\infty}^{\infty} F(r)\exp(iqr)dr, \quad \text{(C1)}$$

$$F(r) = (2\pi)^{-1/2}\int_{-\infty}^{\infty} f(q)\exp(-iqr)dq, \quad \text{(C2)}$$

then it is well known that the Fourier transform of the product $f(q)g(q)$ is given by

$$(2\pi)^{-1/2}\int_{-\infty}^{\infty} f(q)g(q)\exp(-iqr)dq = G(r)\otimes F(r). \quad \text{(C3)}$$

If we set $F(r)=X(r)-iY(r)$, then $X(r)$ is an even function and $Y(r)$ is an odd function,

$$X(r) = (2\pi)^{-1/2}\int_{-\infty}^{\infty} f(q)\cos(qr)dq, \quad \text{(C4)}$$

$$Y(r) = (2\pi)^{-1/2}\int_{-\infty}^{\infty} f(q)\sin(qr)dq, \quad \text{(C5)}$$

and

$$f(q) = (2/\pi)^{1/2}\int_{0}^{\infty} (X(r)\cos qr + Y(r)\sin qr)dr. \quad \text{(C6)}$$

If $f(q)$ is a real odd function,

$$Y(r) = (2\pi)^{-1/2}\int_{-\infty}^{\infty} f(q)\sin(qr)dq$$
$$= (2/\pi)^{1/2}\int_{0}^{\infty} f(q)\sin(qr)dq, \quad \text{(C7)}$$

$$f(q) = (2\pi)^{-1/2}\int_{-\infty}^{\infty} (X(r)\cos(qr) + Y(r)\sin(qr))dr$$
$$= (2\pi)^{-1/2}\int_{-\infty}^{\infty} Y(r)\sin(qr)dr$$
$$= (2/\pi)^{1/2}\int_{0}^{\infty} Y(r)\sin(qr)dr, \quad \text{(C8)}$$

and

$$\int_{-\infty}^{\infty} f(q+q_T)\sin(qr)dq$$
$$= -\mathrm{Im}\left[\int_{-\infty}^{\infty} f(q+q_T)\exp(-iqr)dq\right]$$
$$= -\mathrm{Im}\left[\exp(iq_Tr)\int_{-\infty}^{\infty} f(q)\exp(-iqr)dq\right]$$
$$= -\mathrm{Im}\left[\exp(iq_Tr)\left(-i\int_{-\infty}^{\infty} f(q)\sin(qr)dq\right)\right]$$

$$= \cos(q_T r) \int_{-\infty}^{\infty} f(q)\sin(qr)dq. \tag{C9}$$

If $g(q)$ is a real even function,

$$X(r) = (2\pi)^{-1/2} \int_{-\infty}^{\infty} g(q)\cos(qr)dq$$

$$= (2/\pi)^{1/2} \int_{0}^{\infty} g(q)\cos(qr)dq, \tag{C10}$$

$$g(q) = (2\pi)^{-1/2} \int_{-\infty}^{\infty} (X(r)\cos(qr) + Y(r)\sin(qr))dr$$

$$= (2\pi)^{-1/2} \int_{-\infty}^{\infty} X(r)\cos(qr)dr$$

$$= (2/\pi)^{1/2} \int_{0}^{\infty} X(r)\cos(qr)dr, \tag{C11}$$

and

$$\int_{-\infty}^{\infty} g(q+q_T)\cos(qr)dq$$

$$= \mathrm{Re}\left[\int_{-\infty}^{\infty} g(q+q_T)\exp(-iqr)dq \right]$$

$$= \mathrm{Re}\left[\exp(iq_T r) \int_{-\infty}^{\infty} g(q)\exp(-iqr)dq \right]$$

$$= \mathrm{Re}\left[\exp(iq_T r)\left(\int_{-\infty}^{\infty} g(q)\cos(qr)dq \right) \right]$$

$$= \cos(q_T r) \int_{-\infty}^{\infty} g(q)\cos(qr)dq. \tag{C12}$$

Since $f(q)g(q)$ is an odd function, the SFT of the product $f(q)g(q)$ is given by

$$(2/\pi)^{1/2} \int_{0}^{\infty} f(q)g(q)\sin(qr)dq$$

$$= (2/\pi)^{1/2} \int_{0}^{\infty} (2/\pi)^{1/2} \int_{0}^{\infty} Y(u)\sin(qu)du g(q)\sin(qr)dq$$

$$= (2/\pi) \int_{0}^{\infty} Y(u) \int_{0}^{\infty} g(q)\sin(qu)\sin(qr)dqdu$$

$$= (2/\pi) \int_{0}^{\infty} Y(u) \int_{0}^{\infty} g(q)\tfrac{1}{2}$$

$$\times(\cos(qu-qr) - \cos(qu+qr))dqdu$$

$$= (2\pi)^{-1/2} \int_{0}^{\infty} Y(u)(X(u-r) - X(u+r))du$$

$$= (2\pi)^{-1/2} \left[\int_{0}^{\infty} Y(u)X(u-r)du - \int_{0}^{\infty} Y(u)X(u+r)du \right]$$

$$= (2\pi)^{-1/2} \left[\int_{0}^{\infty} Y(u)X(u-r)du + \int_{-\infty}^{0} Y(u)X(u-r)du \right]$$

$$= (2\pi)^{-1/2} \int_{-\infty}^{\infty} Y(u)X(u-r)du = Y(r) \otimes X(r). \tag{C13}$$

[1] I. I. Vorontsov , A. Y. Kovalevsky, Y. S. Chen, T. Graber, M. Gembicky, I. V. Novozhilova, M. A. Omary, and P. Coppens, Phys. Rev. Lett. **94**, 193003 (2005).
[2] P. Coppens, Chem. Commun. (Cambridge) **2003**, 1317.
[3] P. Coppens and I. V. Novozhilova, Faraday Discuss. **122**, 1 (2003).
[4] K. J. Gaffney, A. M. Lindenberg, J. Larsson *et al.*, Phys. Rev. Lett. **95**, 125701 (2005).
[5] A. M. Lindenberg, J. Larsson, K. Sokolowski-Tinten *et al.*, Science **308**, 392 (2005).
[6] I. V. Tomov, D. A. Qulianov, P. Chen, and P. M. Rentzepis, J. Phys. Chem. B **103**, 7081 (1999).
[7] C. Rose-Petruck, R. Jimenez, T. Guo, A. Cavalleri, C. W. Siders, F. Raksi, J. A. Squier, B. C. Walker, K. R. Wilson, and C. P. J. Barty, Nature (London) **398**, 310 (1999).
[8] A. Plech, S. Kurbitz, K. J. Berg, H. Graener, G. Berg, S. Gresillon, M. Kaempfe, J. Feldmann, M. Wulff, and G. von Plessen, Europhys. Lett. **61**, 762 (2003).
[9] A. Plech, R. Randler, G. Armin, and M. Wulff, J. Synchrotron Radiat. **9**, 287 (2002).
[10] M. Wulff, M. Lorenc, A. Plech, H. Ihee, S. Bratos, F. Mirloup, and R. Vuilleumier, in *Femtochemistry and Femtobiology: Ultrafast Events in Molecular Science*, edited by M. M. Martin and J. T. Hynes (Elsevier, New York, 2004), p. 337.
[11] A. Plech, M. Wulff, S. Bratos, F. Mirloup, R. Vuilleumier, F. Schotte, and P. A. Anfinrud, Phys. Rev. Lett. **92**, 125505 (2004).
[12] H. Ihee, M. Lorenc, T. K. Kim, Q. Y. Kong, M. Cammarata, J. H. Lee, S. Bratos, and M. Wulff, Science **309**, 1223 (2005).
[13] J. Davidsson, J. Poulsen, M. Cammarata *et al.*, Phys. Rev. Lett. **94**, 245503 (2005).
[14] T. K. Kim, M. Lorenc, J. H. Lee *et al.*, Proc. Natl. Acad. Sci. U.S.A. **103**, 9410 (2006).
[15] A. M. Lindenberg, Y. Acremann, D. P. Lowney, P. A. Heimann, T. K. Allison, T. Matthews, and R. W. Falcone, J. Chem. Phys. **122**, 204507 (2005).
[16] M. Cammarata, M. Lorenc, T. K. Kim *et al.*, J. Chem. Phys. **124**, 124504 (2006).
[17] P. Georgiou, J. Vincent, M. Andersson, A. B. Wohrl, P. Gourdon, J. Poulsen, J. Davidsson, and R. Neutze, J. Chem. Phys. **124**, 234507 (2006).
[18] H. Ihee, S. Rajagopal, V. Srajer, R. Pahl, S. Anderson, M. Schmidt, F. Schotte, P. A. Anfinrud, M. Wulff, and K. Moffat, Proc. Natl. Acad. Sci. U.S.A. **102**, 7145 (2005).
[19] F. Schotte, M. Lim, T. A. Jackson, A. V. Smirnov, J. Soman, J. S. Olson, G. N. Phillips Jr., M. Wulff, and P. Anfinrud, Science **300**, 1944 (2003).
[20] E. Collet, M. H. Lemee-Cailleau, M. Buron-Le Cointe *et al.*, Science **300**, 612 (2003).
[21] S. Techert, F. Schotte, and M. Wulff, Phys. Rev. Lett. **86**, 2030 (2001).
[22] J. Larsson, A. Allen, P. H. Bucksbaum *et al.*, Appl. Phys. A: Mater. Sci. Process. **75**, 467 (2002).
[23] G. Busse, T. Tschentscher, A. Plech, M. Wulff, B. Frederichs, and S. Techert, Faraday Discuss. **122**, 105 (2003).
[24] A. M. Lindenberg, I. Kang, S. L. Johnson *et al.*, Phys. Rev. Lett. **84**, 111 (2000).
[25] A. H. Chin, R. W. Schoenlein, T. E. Glover, P. Balling, W. P. Leemans, and V. V. Shank, Phys. Rev. Lett. **83**, 336 (1999).
[26] C. Rischel, A. Rousse, I. Uschmann, P.-A. Albouy, J.-P. Geindre, P. Audebert, J.-C. Gauthier, E. Forster, J.-L. Martin, and A. Antonetti, Nature (London) **390**, 490 (1997).
[27] R. Srinivasan, J. S. Feenstra, S. T. Park, S. Xu, and A. H. Zewail, Science **307**, 558 (2005).
[28] S. T. Park, J. S. Feenstra, and A. H. Zewail, J. Chem. Phys. **124**, 174707 (2006).
[29] F. Vigliotti, S. Chen, C.-Y. Ruan, V. A. Lobastov, and A. H. Zewail, Angew. Chem., Int. Ed. **43**, 2705 (2004).
[30] C.-Y. Ruan, V. A. Lobastov, F. Vigliotti, S. Chen, and A. H. Zewail, Science **304**, 80 (2004).

[31] H. Park, X. Wang, S. Nie, R. Clinite, and J. Cao, Phys. Rev. B **72**, 100301 (2005).
[32] H. Park, X. Wang, S. Nie, R. Clinite, and J. Cao, Solid State Commun. **136**, 559 (2005).
[33] H. Park, S. Nie, X. Wang, R. Clinite, and J. Cao, J. Phys. Chem. B **109**, 13854 (2005).
[34] H. Park, Z. Hao, X. Wang, S. Nie, R. Clinite, and J. Cao, Rev. Sci. Instrum. **76**, 083905 (2005).
[35] J. Cao, Z. Hao, H. Park, C. Tao, D. Kau, and L. Blaszczyk, Appl. Phys. Lett. **83**, 1044 (2003).
[36] B. J. Siwick, J. R. Dwyer, R. E. Jordan, and R. J. D. Miller, Science **302**, 1382 (2003).
[37] R. C. Dudek and P. M. Weber, J. Phys. Chem. A **105**, 4167 (2001).
[38] X. Zeng, B. Lin, I. El-Kholy, and H. E. Elsayed-Ali, Phys. Rev. B **59**, 14907 (1999).
[39] X. J. Wang, D. Xiang, T. K. Kim, and H. Ihee, J. Korean Phys. Soc. **48**, 390 (2006).
[40] H. Ihee, V. A. Lobastov, U. Gomez, B. M. Goodson, R. Srinivasan, C.-Y. Ruan, and A. H. Zewail, Science **291**, 458 (2001).
[41] H. Ihee, J. Cao, and A. H. Zewail, Angew. Chem., Int. Ed. **40**, 1532 (2001).
[42] Q. Y. Kong, J. Kim, M. Lorenc, T. K. Kim, H. Ihee, and M. Wulff, J. Phys. Chem. A **109**, 10451 (2005).
[43] F. Schotte, S. Techert, P. A. Anfinrud, V. Srajer, K. Moffat, and M. Wulff, in *Third-Generation Hard X-ray Synchrotron Radiation Sources*, edited by D. Mills (Wiley, New York, 2002), p. 345.
[44] K. Hoshina, K. Yamanouchi, T. Ohshima, Y. Ose, and H. Todokoro, J. Chem. Phys. **118**, 6211 (2003).
[45] K. Hoshina, K. Yamanouchi, T. Ohshima, Y. Ose, and H. Todokoro, Chem. Phys. Lett. **353**, 27 (2002).
[46] K. Hoshina, K. Yamanouchi, T. Ohshima, Y. Ose, and H. Todokoro, Chem. Phys. Lett. **353**, 33 (2002).
[47] T. S. Dibble and L. S. Bartell, J. Phys. Chem. **96**, 8603 (1992).
[48] J. D. Ewbank, J. Y. Luo, J. T. English, R. Liu, W. L. Faust, and L. Schafer, J. Phys. Chem. **97**, 8745 (1993).
[49] J. C. Williamson, J. Cao, H. Ihee, H. Frey, and A. H. Zewail, Nature (London) **386**, 159 (1997).
[50] S. Bratos, F. Mirloup, R. Vuilleumier, and M. Wulff, J. Chem. Phys. **116**, 10615 (2002).
[51] S. Bratos, F. Mirloup, R. Vuilleumier, M. Wulff, and A. Plech, Chem. Phys. **304**, 245 (2004).
[52] M. Wulff, S. Bratos, A. Plech, R. Vuilleumier, F. Mirloup, M. Lorenc, Q. Kong, and H. Ihee, J. Chem. Phys. **124**, 034501 (2006).
[53] M. J. Frisch, G. W. Trucks, H. B. Schlegel *et al.*, GAUSSIAN 03, Gaussian, Inc., Pittsburgh, PA, 2003.
[54] H. Ihee, A. H. Zewail, and W. A. Goddard III, J. Phys. Chem. A **103**, 6638 (1999).
[55] B. E. Warren, *X-ray Diffraction* (Dover, New York, 1990).
[56] A. Guinier, *X-Ray Diffraction: In Crystals, Imperfect Crystals, and Amorphous Bodies* (Dover, New York, 1994).
[57] I. Hargittai and M. Hargittai, *Stereochemical Applications Of Gas-Phase Electron Diffraction* (VCH, New York, 1988).
[58] U. Banin and S. Ruhman, J. Chem. Phys. **98**, 4391 (1993).
[59] T. Kuhne and P. Vohringer, J. Phys. Chem. A **102**, 4177 (1998).
[60] M. T. Zanni, B. J. Greenblatt, A. V. Davis, and D. M. Neumark, J. Chem. Phys. **111**, 2991 (1999).
[61] D. A. Mcquarrie, *Mathematical Methods for Scientists and Engineers* (University Science Books, Sausalito, CA, 2003).